Modelling heat flow in a cold, high altitude glacier: Interpretation of measurements from Colle Gnifetti, Swiss Alps

Martin P. Lüthi, Martin Funk

Versuchsanstalt für Wasserbau, Hydrologie und Glaziologie (VAW), Zürich, Switzerland

Modelling the heat flow in small, cold high altitude glaciers is important for the interpretation of paleoclimatic data from ice cores. Coupled glacier flow and heat flow models are presented, which incorporate the firn densification, the heat advection and possible phase transitions at the permafrost boundaries within the bedrock.
Marked bends observed in the temperature profiles from two recent boreholes on Colle Gnifetti are interpreted with help of a transient heat flow model, driven with a temperature history. The conclusion is, that substantial warming of the mean firn temperature in shallow depths has taken place over the last decades. This has not been observed so far in cold firn regions of the Alps.
Modelled heat fluxes in the massif of Monte Rosa are strongly influenced by the mountain topography. This leads to a spatial variability of the temperature gradient near the glacier base which has been observed in boreholes to the bedrock. In order to match the measured temperature profiles in the glacier, the vertical heat flux in great depths has to be set to an extremely low value. It is shown with help of the transient heat flow model that this is a paleoclimatic effect, possibly enhanced by a degrading permafrost base.

1 Introduction

Small, cold high altitude glaciers react very sensitive to variations in the surface energy balance. Low ice thicknesses (typically 50 to 100 m) and a high accumulation rates (typically $0.2-5\,\mathrm{m\,a^{-1}}$ w.e.) rapidly advect temperature changes of the firn near the surface into the body of the glacier. Through the temperature dependence of the firn viscosity, deformation rates and thus the flow field are influenced. Even more dramatic changes occur if basal boundary conditions are affected, especially if patches previously frozen to the bedrock become temperate. Under these conditions basal sliding may alter the flow field. Under certain circumstances, large ice avalanches can be the consequence of a reduced stabilisation at the glacier base (Röthlisberger, 1981, 1987; Margreth and Funk, 1999).

Ice cores from several cold Alpine high altitude glaciers have been investigated in order to reconstruct the climatic history of the past (Oeschger and others, 1977; Schotterer and others, 1985; Wagenbach and others, 1988; Döscher and others, 1996; Schwikowski and others, 1999a, 1999b; de Angelis and Gaudichet, 1991; Vincent and others, 1997). The interpretation of the information obtained from these cores relies on the assumption, that ice temperatures were cold throughout the period investigated. Detailed modelling of the heat flow and the ice advection provide the required information. Moreover, such models provide an independent dating of the ice cores, based on the modelled ice flow only.

The analysis of heat flow processes in high altitude glaciers is complicated by several factors, each of which requires careful treatment:

- The complex surface and bedrock geometries of the glacier induce complex ice flow patterns.

- The thermal and mechanical properties of firn depend strongly on firn density.
- Surface boundary conditions vary strongly with topography (exposition, surface inclination and altitude). Typically these boundary conditions are only poorly determined and have to be estimated.
- The mountain topography leads to non-vertical heat fluxes in the bedrock, especially near mountain tops and free rock faces.
- A seasonal snow cover of rock faces further complicates the treatment.
- The long term temperature history affects the heat fluxes at depth.
- Permafrost conditions prevail within the upper parts of the mountains. Phase transitions due to thawing and freezing water at the permafrost boundaries cannot be neglected in transient calculations.

Most of the problems outlined above have been individually addressed in previous studies. In this paper we demonstrate the application of numerical models to the joint solution of the heat advection-diffusion problem including effects of latent heat. The calculation of the velocity field and the density distribution within the glacier is achieved with a flow model including firn deformation and firn compaction. Except for the precise boundary conditions, all problems are physically correctly addressed. As an application of the models, recent temperature records in two boreholes to the bedrock on Colle Gnifetti (Monte Rosa, Swiss Alps) are discussed.

2 Heat flux in mountains

Glaciers located on mountains with a pronounced topographic relief are subject to the influence of a spatially varying, non-vertical heat flux at the glacier base. These variations of heat fluxes are a consequence of the often complicated temperature distribution within the mountain, which is caused by the strong variation of boundary conditions in both space and time. The rock face exposition, seasonal shading effects and a varying snow cover contribute to this pattern. Only at very large depths (several kilometres) the geothermal heat fluxes are unaffected by the mountain topography. In contrast, temperature gradients are mainly perpendicular to the surface near free mountain faces.

The temperature field and associated heat fluxes in a mountain ridge have been investigated in detail, revealing the above mentioned influences as well as the importance of phase transitions of vein water in the rock near the surface (Wegmann and others, 1998). In a modelling study of a ridge with two faces of different exposition (North and South), predominantly horizontal heat fluxes have been obtained. Snow patches and glaciers further complicate this heat flow pattern as they often act as a heat source (through refreezing meltwater) in an otherwise cold mountain face.

It is well established that temperatures at depth are a consequence of the temperature history over thousands of years. In addition to the well known process of heat diffusion, the possibility of phase transitions at the permafrost boundaries has to be considered. Assuming a moisture content of several percent, the transient degradation of permafrost consumes an important part of the geothermal heat flux (Wegmann and others, 1998). Inversely, a cooling condition causes additional water to freeze, thus releasing heat and adding to the geothermal heat flux.

3 Field equations

The quantitative analysis of the processes outlined in the introductory section of this paper requires the solution of a coupled system of equations for the balances of mass, linear momentum and energy. The mathematical formulation of the slow flow of an isotropic, viscous, compressible, heat-conducting fluid (i.e. firn) is formulated in the Eulerian description and reads (Malvern, 1969; Hutter, 1983)

$$\frac{\partial \rho}{\partial t} + \nabla(\rho \mathbf{v}) = 0\,, \tag{1a}$$

$$\nabla \sigma + \rho \mathbf{g} = 0\,, \tag{1b}$$

$$\rho C \left(\frac{\partial T}{\partial t} + \mathbf{v} \nabla T \right) = \nabla(k \nabla T) + \mathrm{tr}\,(\sigma \dot{\epsilon}) + Q_f\,. \tag{1c}$$

Here ρ is the density, $\mathbf{v}$ the velocity vector, σ the stress tensor, $\mathbf{g}$ the gravitational body force, $\dot{\epsilon}$ the strain rate tensor and C the heat capacity. The acceleration term is omitted in equation (1b), which may be established with a scaling argument (Hutter, 1983). The Fourier law of heat conduction $\mathbf{q} = -k \nabla T$ has been used, where k is the thermal conductivity. Heat sources are the dissipative heat production $\mathrm{tr}\,(\sigma \dot{\epsilon})$ during deformation and the release of latent heat Q_f during freezing. It is assumed that no transport of moisture occurs. The equation system is closed by a constitutive equation for the firn, relating the stress tensor to the strain rate tensor.

The equation system (1) is coupled through temperature and density. The evolution of these quantities is given by equations (1a) and (1c), and they appear as state variables in the constitutive equation (3). Moreover, the thermal conductivity k is strongly dependent on density and, to a lesser extent, on temperature.

4 Numerical solution

The solution of equations (1) for a given geometry requires numerical analysis. Since the glacier flow and the heat diffusion processes are interdependent, a coupled mechanical and thermal analysis is needed. This coupling is achieved with independent Finite Element models for firn densification (Equation 1a), glacier flow (1b) and heat flow (1c).

A steady state solution of equations (1a) and (1b) for given firn temperatures has been calculated with coupled models of glacier flow and firn densification in three dimensions (Lüthi and Funk, 2000). The coupling of both models has been achieved with a fixed point iteration. The prescribed firn temperatures were interpolated from the measured borehole temperatures. Resulting firn densities closely match the densities measured on ice cores.

In this paper we discuss the transient solution of equations (1b) and (1c) along a flow line. The firn densities are taken from the 3D model discussed above (Lüthi and Funk, 2000) and are assumed constant with time. The ice flow model depends on the temperature field calculated with the heat flow model, which on the other hand requires output quantities from the flow model such as the ice velocity and the dissipative heat production. This coupling is again achieved through iterative use of both models.

4.1 Glacier flow model

The glacier flow model is based on a flow law of firn. This flow law includes the firn compressibility as well as the density dependent variation of firn viscosity. The flow law is formulated

in terms of an isotropic, viscous, compressible fluid, where effective viscosities are dependent on the stress state and on temperature and density as scalar state variables. In the limit of full density this constitutive equation should take the form of a power law fluid (i.e. Glen's flow law).

Denoting the stress tensor by σ_{ij}, the mean stress is $\sigma_m := \frac{1}{3}\sigma_{kk}$ and the stress deviator tensor is $\sigma'_{ij} := \sigma_{ij} - \sigma_m$. Glen's flow law is written as

$$\dot{\epsilon}_{ij} = A_0 B(T) \tau^{n-1} \sigma'_{ij} \,, \tag{2}$$

where A_0 and n are flow law parameters and the effective shear stress is defined by $\tau^2 := \frac{1}{2}\sigma'_{ij}\sigma'_{ij}$. It is assumed that the temperature dependence may be separated into a multiplicative factor $B(T)$.

The flow law for firn extends equation (2) to include a compressible part proportional to σ_m (Sofronis and McMeeking, 1992; Duva and Crow, 1994; Cocks, 1994). Two parameters $a(D)$ and $b(D)$ describing the influence of the relative firn density $D = \rho/\rho_{\text{ice}}$ (where $\rho_{\text{ice}} = 917\,\text{kg}\,\text{m}^{-3}$) are introduced. The strain rates $\dot{\epsilon}_{ij}$ depend on the stress deviator tensor σ'_{ij} and the mean stress σ_m according to the relation

$$\dot{\epsilon}_{ij} = A_0 B(T) \sigma_D^{n-1} \left\{ a(D)\sigma'_{ij} + \frac{2}{3} b(D) \sigma_m \delta_{ij} \right\}, \tag{3}$$

where the stress invariant σ_D is defined as

$$\sigma_D^2 := a(D)\tau^2 + b(D)\sigma_m^2 \,. \tag{4}$$

In the limit of full density ($D \to 1$) the contribution of the compressible part must vanish so that Glen's flow law is recovered. These requirements restrain the limiting behaviour of the parameters to

$$a(D) \overset{(D\to 1)}{\longrightarrow} 1 \quad \text{and} \quad b(D) \overset{(D\to 1)}{\longrightarrow} 0 \,. \tag{5}$$

The detailed form of this parameterisation for firn has been given by Gagliardini and Meyssonnier (1997). This flow law has been implemented in the finite element code MARC (MARC, 1997; Lüthi and Funk, 2000). Eight node isoparametric quadratic elements with Galerkin weighting have been used in the two-dimensional streamline model discussed in this paper.

4.2 Heat flow model

Steady state and transient situations are modelled with the heat transfer code of MARC, which includes a streamline-upwind Petrov-Galerkin (SUPG) weighting (Zienkiewicz and Taylor, 1989; MARC, 1997). Eight node isoparametric quadratic heat transfer elements are used. Required input quantities such as the velocity field and internal heat sources are provided by the mechanical analysis.

4.3 Latent heat

Freezing and thawing of moisture with production or consumption of latent heat are important effects which have to be taken into account. The treatment of the phase transition requires to exactly locate the phase boundary surface and to apply an additional internal boundary condition. This approach has been worked out successfully for the finite difference method (Funk and others, 1994). However, the application of this approach within the finite element

method would require the extensive use of remeshing in order to match the transition surface with element boundaries. An alternative, simple continuum approximation has been used in the heat flow model, which can readily be used within the finite element method.

We assume that the phase transition occurs within a temperature interval between the (colder) solidus temperature T_s and the (warmer) liquidus temperature T_l. The amount of heat released during freezing then is

$$Q = L + \frac{(C_i + C_w)}{2}(T_l - T_s)\,, \tag{6}$$

where L is the latent heat of freezing, C_i and C_w are the heat capacities of ice and water (in units of $\mathrm{J\,kgK^{-1}}$), and we assume that the amount of freezing water varies linearly with temperature. Thus we arrive at an effective heat capacity during freezing of

$$C^\star = \frac{L}{T_l - T_s} + \frac{(C_i + C_w)}{2}\,. \tag{7}$$

The volumetric heat capacity $c = \rho C$ (in units of $\mathrm{J\,m^{-3}K^{-1}}$) of rock with a moisture content w (volume fraction) is then given by

$$c = \begin{cases} (1-w)c_r + wc_i, & T < T_s \\ (1-w)c_r + wc^\star, & T_s \le T < T_f \\ (1-w)c_r + wc_w, & T \ge T_f\,. \end{cases} \tag{8}$$

This approximate approach is physically justified if the phase transition surface is located within the bedrock (which is the case in the present study). Due to the capillary nature of the rock veins and cracks, the phase transition does not occur at a single temperature but in a temperature interval of about 0.3 K (Wegmann and others, 1998). A similar argumentation has also been put forward for glacier ice (Lliboutry, 1993).

5 A case study of Colle Gnifetti

The methods outlined in the previous sections are used to interpret temperature measurements from two boreholes on Colle Gnifetti (Monte Rosa, Swiss Alps). Colle Gnifetti is the uppermost part of the accumulation area of Grenzgletscher, forming a saddle between Zumsteinspitze and Punta Gnifetti of Monte Rosa, at an altitude of 4400-4550 m a.s.l.. The ice flows from both peaks to the main outflow of Grenzgletscher, or breaks off over a steep ice cliff on its north-eastern margin (Figure 1). Measured accumulation rates are between 0.2 and 1.1 $\mathrm{m\,a^{-1}}$ w.e. with very strong spatial and temporal variations due to the wind exposed location. The glacier is located between the recrystallisation-infiltration zone and the cold infiltration zone (Alean and others, 1983). Meltwater produced occasionally by intense solar radiation at elevated air temperatures refreezes some centimetres below the surface. Measured ice temperatures never exceed the range between -9°C and -14°C (Oeschger and others, 1977; Alean and others, 1983; Haeberli and Funk, 1991; Lüthi, 1999).

A basal temperature of -12.3°C and a temperature gradient of 19 $\mathrm{mK\,m^{-1}}$ have been measured in the 120 m deep borehole `B82-1` (located in the saddle canter, Figure 1) in 1982. The temperature profile from this borehole closely matched a modelled steady state temperature profile (Haeberli and Funk, 1991). Contrary to observations in the Arctic, no influence of the warming since the beginning of the 20th century was discernible. This observation will be further investigated in Section 6.4.

Firn temperatures measured in shallow (2 m) holes vary up to 6°C within 400 m horizontal distance (Alean and others, 1983). Only a small variation of the firn temperature was observed

within the north-exposed slope between Punta Gnifetti and the saddle canter. In contrast, near surface firn temperatures substantially increased on the south-exposed slope towards Zumsteinspitze (Haeberli and Alean, 1985). This is obviously due to enhanced net radiation, which was corroborated by the increased number of melt layers.

5.1 Borehole temperature measurements

In 1996/97, we performed new temperature measurements in two deep boreholes drilled in 1995 by the Universities of Heidelberg and Berne. Five thermistors were installed in the 62 m deep hole `B95-1` and seven in the 101 m deep hole `B95-2` with a vertical spacing varying from 5 to 20 m (see Figure 1 for the location of these boreholes).

Thermistors of negative temperature coefficient (NTC) type (Fenwal 197-103 LAG-A01) were sealed into nearly fitting aluminium tubes in order to keep the influence of pressure and humidity low. The thermistors were soldered to individual two-conductor cables and were waterproofed by heat-shrink tubing. All thermistors were individually calibrated at 7 reference temperatures in the range of -17°C to 5°C in a bath of a mixture of water and anti-freeze. The calibration was performed with connected cables in exactly the same configuration and with the same digital multimeter used in the field. Four reference thermistors, calibrated to an absolute accuracy of 20 mK by the Swiss Federal Office of Metrology, were used to determine the homogeneity and the absolute value of the bath temperature. The accuracy of measured temperatures is better than 50 mK over the temperature range -15°C to -10°C encountered in the glacier. Relative temperature changes at a single thermistor may be as accurate as 20 mK.

Thermistors were installed in both boreholes in June 1996, one year after completion of the drilling. We therefore assume that borehole temperatures reached an undisturbed state. Four to five readings were taken between June 1996 and October 1997. Borehole temperatures from thermistors installed below the zone of annual variation (below 15 m) are shown in Figure 2. Measured temperatures are between -12.4°C and -13.5°C and lie within the range of previous measurements.

A slight warming of most thermistors has been observed, with warming rates of up to 70 mK a^{-1} at thermistors between 20 and 30 m depth. A possible misinterpretation due to stretching of the thermistor cables during ice motion is improbable and would result in a higher resistivity, and therefore in apparent colder temperatures. A warming of the thermistors should be expected as they move downwards with the firn. An estimate of this effect for the thermistors with the largest warming rates in borehole `B95-2` gives warming rates of 4 to 8 mK a^{-1}, which is considerably smaller than the measured warming rates. The warming of the firn is further corroborated by the striking bend of the temperature profile to warmer temperatures which is clearly visible in borehole `B95-2` at a depth of 30 m (Figure 2). Such a feature has not been observed in Alpine glaciers up to date (Haeberli and Funk, 1991).

From these observations we conclude that the measurements indicate a warming of the firn in a non-steady situation. Similar temperature profiles exhibiting a bend towards warmer temperatures have been measured some decades ago on White Glacier (Axel Heiberg Island, Canadian Arctic; Blatter, 1987; Blatter and Kappenberger, 1988). The shapes of these temperature profiles have been reproduced with a heat flow model and a prescribed surface temperature history. We aim at a similar modelling study in this paper, which will take into account the topographic influence of the Monte Rosa massif.

5.2 Temperature gradients and heat fluxes

Temperature gradients from three deep boreholes are plotted in Figure 2. Both deep boreholes B82-1 and B95-2 in the central saddle area exhibit temperature gradients of $18 - 19\,\mathrm{mK\,m^{-1}}$, whereas they reach $22 - 25\,\mathrm{mK\,m^{-1}}$ in borehole B95-1. Two boreholes drilled in 1977 (B77) exhibit similar temperature gradients, however they also reach only relatively shallow depths of 30 and 50 m, compared to an ice thickness of 120 m (Oeschger and others, 1977).

An inspection of the location of the drill sites (Figure 1) reveals, that boreholes with higher temperature gradients are relatively close to the ice cliff on the north-eastern side (boreholes B77-1 and B77-2) or to the steep south-western face of Monte Rosa (borehole B95-1). Thus the influence of these rock walls, which are exposed to the atmosphere and solar radiation, is clearly manifested in the temperature gradients. Wegmann (1998) showed that irradiated mountain slopes strongly influence the heat fluxes and therefore the temperature distribution in a mountain top. The observed temperature gradients are interpreted to reflect the consequences of this result.

Heat fluxes are calculated from the measured temperature gradients using a density dependent thermal conductivity. Two different relations are used as a lower and upper limit (the relations of van Dusen and Schwerdtfeger, cf. Appendix). The heat fluxes calculated with these relations and evaluated with the respective density profiles are shown in Figure 2. Calculated basal heat fluxes are between $35 - 40\,\mathrm{mW\,m^{-2}}$ for both saddle boreholes B82-1 and B95-2 and increase to $40 - 45\,\mathrm{mW\,m^{-2}}$ for borehole B95-1. Geothermal heat flux is estimated to be roughly $70\,\mathrm{mW\,m^{-2}}$ at sea level in the Monte Rosa area (Medici and Rybach, 1995). Such a decrease of the vertical heat flux may be expected, as the temperature field in the upper part of high mountains is strongly influenced by lateral heat fluxes from exposed slopes. This is further investigated in Section 6.

5.3 Modelled flow velocities

The flow velocities of Colle Gnifetti have been modelled along a flowline as well as in three dimensions (Lüthi and Funk, 2000). For the purpose of this study we concentrate on the two dimensional flow model along an approximate flowline, shown in Figure 3. Starting below Punta Gnifetti, it passes through the borehole locations B95-1, B82-2 and B95-2 (thick dashed line in Figure 1) and ends at the big crevasse in the outflow to Grenzgletscher. The bedrock depth is well known from a radar profile and surface velocities have been measured at nine stakes.

Ages of chemically dated layers in ice cores, firn density profiles as well as surface velocities measured at nine stakes on the flowline have been reproduced by the flow model (Lüthi and Funk, 2000). While it is clear that a flowline model is a poor approximation in the downstream part of the model geometry where ice flow is largely influenced by the topography in three dimensions, it is likely to be a reasonable approximation of the ice flow in the upper part of the glacier, i.e. upstream of borehole B95-2.

The flow velocities calculated with the flowline model are plotted on several cross sections in Figure 3. The comparison with velocities measured at nine stakes shows a good agreement in the region between the boreholes. A noteworthy feature is the unusual shape of the velocity profiles with an increasing horizontal velocity near the surface. This is a consequence of the low viscosity of the firn layer. Substantial deviations occur towards the left model margin because of the curvature of the flowline and undetermined boundary conditions at a big crevasse.

6 Heat flow model

In the present study we concentrate on the principal effects of heat fluxes within a mountain on a small, cold glacier. The model geometry is a two-dimensional cross-section through the Monte Rosa massif including the Colle Gnifetti glacier on the top (the modelled flow line is indicated with a dashed line in Figure 1). The model geometry shown in Figure 4 includes the whole massif of Monte Rosa and reaches down to sea level. The grid of the heat flow model is indicated, and matches that of the mechanical flow line model within the glacier (Figure 3 and shaded area in Figure 4; Lüthi and Funk, 2000).

An implementation of a similar model in three dimensions would pose no additional difficulties. A glacier flow model including the firn rheology has been successfully implemented (Lüthi and Funk, 2000), and the solution of the heat diffusion-advection equation is a standard capability of most finite element codes. The main problem is to provide accurate thermal boundary conditions on the glacier surface as well as on the rock walls.

6.1 Thermal conductivities

The specific heat capacity C and the thermal conductivity k of firn are both density and temperature dependent and are appropriately parameterised (cf. Appendix). Since it is difficult to determine from the measurements which formula should be preferred, an average conductivity is used.

The thermal properties of the bedrock are not known. Thermal conductivities of gneiss show large variations, mainly due to anisotropy and are usually in the range of 2.5 to $3.5\,\mathrm{W\,m^{-1}\,K^{-1}}$ (Clauser and Huenges, 1995). A thermal conductivity of $3.2\,\mathrm{W\,m^{-1}\,K^{-1}}$ has been measured in frozen, water saturated samples of gneiss from a high Alpine site (Wegmann, 1998). Since the upper 1000 m (at least) of Monte Rosa are in permafrost conditions, a value of $3.2\,\mathrm{W\,m^{-1}}$ is adopted throughout this study. The volumetric heat capacity is assumed to be $2063\,\mathrm{kJ\,m^{-3}\,K^{-1}}$ (Wegmann, 1998).

6.2 Boundary conditions

Thermal boundary conditions are not well known for high altitude glaciers and rock walls. Consequently, simple parameterisations are used in this study. A mean firn surface temperature is used in order to hide the details of the complex heat and mass exchange processes at the firn surface. The mean firn temperature at the glacier surface is set to $T_{\mathrm{surf}} = -14.1°\mathrm{C}$ (this was also the 10 meter firn temperature in the southern part of Colle Gnifetti in 1985; Haeberli and Funk, 1991). A decrease of surface temperatures in the steep slope towards Punta Gnifetti is plausible due to reduced solar radiation caused by a shading effect. Hence a horizontal gradient of the surface firn temperature of $-0.02°\mathrm{C\,m^{-1}}$ is prescribed from the canter between the boreholes (at coordinate 300 m in Figures 3 and 4) in the upstream direction towards the top of Punta Gnifetti. This boundary condition is applied along the edge of the model indicated with T_{surf} in Figure 4. On the south face of Monte Rosa (T_{south} in Figure 4) parameterised thermal boundary conditions are chosen according to Wegmann (1998, p. 102), namely a surface temperature depending on altitude z of $T_{\mathrm{south}}(z) = 13.0°\mathrm{C} - z \cdot 0.0045°\mathrm{C\,m^{-1}}$ (a nearly identical parameterisation was given by Rybach and Pfister (1994) for the south side of the Alps). No horizontal heat fluxes are admitted on the left boundary and on the lower half of the right boundary of the model geometry ($q = 0$ in Figure 4). A vertical heat flux of $70\,\mathrm{mW\,m^{-2}}$ (Medici and Rybach, 1995) was initially prescribed at sea level (lower model boundary). As will be shown, this heat flux

only leads to reasonable results in a transient model including the effects of latent heat within the bedrock.

6.3 Steady state solutions

The calculated steady state temperature profiles are shown in Figure 5. A reasonable agreement with the measured temperatures (Section 5.1) is obtained for the lower part of the boreholes. The temperature gradients in the bottom part of both boreholes can only be reproduced by setting the basal heat flux at sea level to a value of $q \leq 20\,\mathrm{mW\,m^{-2}}$. This surprisingly low value may be an effect of several processes and must therefore not be taken literally. In fact, the whole complexity of the three dimensional geometry, the geology, eventual effects of hydraulic active systems and radiative heat sources strongly influence the heat fluxes in the alpine massifs (Busslinger, 1998). Additionally, the effects of latent heat have to be taken into account near the rock surface and at the permafrost base, which is estimated to be at least 1000 m below the glacier. One might speculate that a thawing permafrost base consumes a large part of the geothermal heat flux. For the purpose of obtaining reasonable steady state temperature profiles, the vertical heat flux at sea level has been set to $20\,\mathrm{mW\,m^{-2}}$ in this and the next section. Also the marked bends observed in the upper part of the temperature profiles cannot be explained with the steady state model. These issues will be further investigated in Section 6.4 with a transient heat flow model.

The modelled steady state temperature profiles show a noteworthy feature. While profile `B95-2` is curved in the positive direction, profile `B95-1` exhibits the opposite curvature. The fact that steady state temperature profiles from two neighbouring locations are different in shape demonstrates the necessity to take into account the horizontal and vertical advection and accurate boundary conditions. Also the heat fluxes at the glacier base differ considerably, as they are affected by the free south-east and north-east faces of Monte Rosa. Borehole `B95-1` which is closer to the south-east face shows a temperature gradient which is enhanced by about 25% with respect to borehole `B95-2`. This feature was already detected in the temperature measurements (Figure 2).

6.4 Transient solutions

All surface temperatures ($T_{\mathrm{surf}}(t)$ and $T_{\mathrm{south}}(t)$ in Figure 4) are varied according to the difference of mean annual air temperature with respect to the secular mean temperature (Figure 6). This relies on the assumption that the processes of heat exchange at the surface show the same variation with time as the monthly mean air temperature. Measured temperatures since 1850 from the nearby Grand St. Bernard meteorological station (2479 m a.s.l., some 50 km apart) are used (data from Schüepp, 1961, and from "Annalen der SMA", doubly smoothed with a 9 year running mean). Starting with a steady state in the year 800 and including the medieval climatic optimum and the little ice age, this is a rough approximation to the reconstructed temperature history (von Rudloff, 1980).

Results from the transient model runs are shown in Figure 7. A very good agreement with measurements is obtained for the curvature of profile `B95-2` as well as for the heat fluxes at the glacier base. Modelled temperatures are too low by 0.2°C in the upper part of borehole `B95-1`. This discrepancy could in principle be accounted for with an appropriate parameterisation of surface temperatures upstream of the borehole. We feel that such a matching procedure is of little significance, and therefore prefer a simple parameterisation of the surface temperature.

With a prescribed constant surface temperatures of $T_{\text{surf}} = -13.7°\text{C}$, the temperature profile in borehole `B95-2` is exactly obtained while the temperatures of `B95-1` are too high by about 0.6°C. The results shown in Figure 7 have been obtained with a horizontal temperature gradient of $-0.005°\text{C}\,\text{m}^{-1}$ upstream of the canter between the boreholes (i.e. starting at 300 m in the model geometry of Figures 3 and 4).

6.5 Effects of latent heat

A suspiciously low vertical heat flux at sea level had to be set as boundary condition of the heat flow model in order to reproduce the temperature gradients measured at the base of the glacier. It was speculated in Section 6.3 that this could be an effect of latent heat consumed by thawing permafrost. An investigation of the importance of latent heat requires the modelling of a very long time span in order to obtain the appropriate transient response. Starting the model run at steady conditions some 1200 years ago (as has been done in Section 6.4) cannot reproduce the effects of permafrost degradation, since a temperature change at the surface only penetrates some 100 m during this period. Therefore starting with a steady state, the surface temperature history for the last 20'000 years was prescribed (von Rudloff, 1980). The vertical heat flux at sea level was set to its initial value (Section 6.2) of $70\,\text{mW}\,\text{m}^{-2}$ (Medici and Rybach, 1995). A moisture content of 3 % (volume fraction) throughout the rock was taken as a reasonable value to investigate the principal effects (Wegmann, 1998).

The modelled temperature distribution within the mountain in 1997 is shown in Figure 8. The influence of the south-eastern face (right model boundary) on the temperature distribution results in dipping contour lines. Contour lines nearly parallel to the surface indicate high lateral heat fluxes near the top of the mountain. The time evolution of temperature and vertical heat flux are plotted in Figure 9 for a vertical profile (indicated with an arrow in Figure 8). A kink in the 1997 temperature profile is visible in Figure 9a at the calculated permafrost base. The vertical heat flux within the mountain diminishes from $70\,\text{mW}\,\text{m}^{-2}$ at sea level to $20\,\text{mW}\,\text{m}^{-2}$ in the permafrost zone above 2900 m a.s.l. (Figure 9b). This is due the thawing permafrost base which consumes a large fraction of the geothermal heat flux. The effect of the mountain topography alone can be inferred from Figure 9d which shows model results obtained for dry rock. Due to the absence of the phase transition, the minimum heat fluxes occur at a higher altitude of 3700 m a.s.l.. Above this altitude, both temperature and heat flux profiles are similar and mainly affected by the mountain topography and the applied boundary conditions. Based on the measurements it is impossible to decide on the importance of the latent heat effects. In any case, the low vertical heat flux is the result of the paleoclimatic evolution.

6.6 Discussion of model results

The transient heat flow model is capable to reproduce measured temperature profiles and warming rates in two boreholes on Colle Gnifetti. It has been shown that the measured temperature profiles cannot be obtained with the assumption of a steady state (except perhaps for a strange variation of prescribed surface temperatures). Both borehole temperature profiles exhibit the warming trend which has been observed at the Grand St. Bernard meteorological station. This is mainly caused by the exceptionally high temperatures prevailing since 1980 (Figure 6). A comparison of the modelled temperature profiles in Figure 7 shows that they were close to a steady state profile in 1982. This was also the conclusion of a modelling study (Haeberli and Funk, 1991) in which the temperatures measured in 1983 in borehole `B82-1` were interpreted. The bend in the profile evolved only in the last decade and could not be observed before.

In Figure 10 the time evolution of modelled englacial temperatures at four depths is shown. An important result for the interpretation of the ice cores is that the firn temperatures never exceeded −11°C in the past. Temperature gradients were "normal" (i.e. the surface exhibits always the coldest temperatures) during most of the history. Even at warming rates of one degree per century the borehole temperature profiles show no inversion. Only for extremely fast and large temperature increases a slight inversion can be observed in borehole `B95-2` in 1865 and 1950. The strongest warming occurred during the last 15 years with a surface temperature increase of 1.3°C. Consequently the inversion of the temperature profile encountered in Figure 7 is a very recent effect and is likely to fade away in the near future if the warming trend stops.

6.7 Future evolution

Given the large variability of englacial temperatures within such small high altitude glaciers and the ongoing climate warming, the future evolution of the firn temperatures is of high interest. With increasing firn temperatures, the suitability of Colle Gnifetti as a climate archive could become questionable, since diffusion of chemical species and surface melt events will increase. Two simple scenarios for the next 50 years are discussed to obtain an estimate of the firn temperatures with special attention to the change of basal boundary conditions.

The temperature profiles shown in Figure 11 have been obtained under the assumption of constant surface temperatures during the next 50 years. The bend towards warmer temperatures near the surface fades out after some 30 years and both profiles tend to a steady state. A considerable basal warming of nearly 0.35°C is predicted for borehole `B95-1` and 0.2°C for `B95-2`. Forcing the surface with a one degree warming in the next 50 years, englacial temperatures would increase at a similar rate (Figure 12). The temperature minimum moves downwards in borehole `B95-2` which is caused by the strong vertical advection. The basal warming during the next 50 years is predicted to be 0.5°C and 0.3°C, respectively.

The expected change of basal temperatures will only marginally affect the flow behaviour of Colle Gnifetti, since the glacier will still be frozen to the bedrock. However, the above results hint to an important influence on glaciers with basal temperatures close to the melting point.

7 Conclusions

In this paper we demonstrated the application of combined numerical models of glacier flow and heat flow to interpret borehole temperature measurements from Colle Gnifetti. The models include the ice advection, possible phase transitions at the permafrost base within the mountain as well as the firn compressibility. The following conclusions concerning thermal conditions of cold high altitude glaciers can be drawn:

- The shape of steady temperature profiles depends critically on accumulation, ice advection, the density profile and the spatial distribution of surface temperatures. The influence is so important that curvature of a steady state temperature profile can be both convex or concave.
- Observed differences of basal temperature gradients are caused by the mountain topography, i.e. nearby rock walls.
- Marked bends observed in temperature profiles can be explained with air temperature variations recorded at a nearby meteorological station. Such a close correlation between

surface firn temperature and air temperature is presumably only possible at cold temperatures ($-13°$C).

- Heat fluxes at the glacier base are different from the average heat fluxes at great depths. This is due to the mountain topography as well as the long term climate history.
- Freezing and thawing of moisture within the bedrock strongly affects the heat fluxes.
- Basal temperatures are expected to change considerably in the near future.

A continuation of the ongoing warming trend will raise firn temperatures substantially in the next decades. This will alter the flow pattern of glaciers with temperatures close to the melting point, especially as parts of the glacier bed become temperate. Glaciers terminating in ice cliffs are likely to enhance their ice avalanche activity. In some special cases the stability of whole parts of such glaciers can be affected, resulting in huge ice avalanches.

Detailed studies of surface energy exchange processes are necessary to provide accurate boundary conditions for the heat flow model. Results of the ongoing EC project ALPCLIM will contribute to this knowledge and provide more detailed information on the surface temperature distribution on Colle Gnifetti. In the same context, a systematic monitoring of englacial temperatures will improve our knowledge on the ongoing temperature changes of cold glaciers in the Alps.

Acknowledgements

The field work under sometimes adverse conditions was supported by M. Wegmann, U.H. Fischer, L. Keck, E. Kuriger and R. Zergenyi. We appreciate the collaboration with the group of D. Wagenbach (University of Heidelberg). Many thanks are due J. Luthiger and C. Senn for carefully manufacturing the mechanical and the electronic part of the equipment. Helpful comments of J. Meyssonnier, S. Suter and an anonymous referee improved the clarity of the presentation. This project was funded by ETH research grant No 0-20-982-95.

Appendix: Thermal properties of firn

Specific heat capacity

The specific heat capacity of firn and ice (neglecting the heat capacity of the interstitial air) is dependent on (absolute) temperature T (Paterson, 1994)

$$C = (152.5 + 7.122\,T)\ \mathrm{J\,kg^{-1}\,K^{-1}}\,. \tag{9}$$

Thermal conductivity

The dependency on absolute Temperature T of the thermal conductivity of ice k_{ice} is expressed as an Arrhenius relation (Paterson, 1994)

$$k_{\mathrm{ice}} = 9.828 \exp\left(-5.7 \cdot 10^{-3} T\right)\ \mathrm{W\,m^{-1}\,K^{-1}}\,. \tag{10}$$

It is assumed in this study that the thermal conductivity of firn shows the same temperature dependence, which is taken into account with a multiplicative factor in the equations below.

The thermal conductivity is also strongly dependent on density ρ (Van Dusen, 1929; Schwerdtfeger, 1963; as cited in Paterson, 1994), namely

$$k_{\text{van Dusen}} = 2.1 \cdot 10^{-2} + 4.2 \cdot 10^{-4}\rho + 2.2 \cdot 10^{-9}\rho^3\,, \tag{11}$$

$$k_{\text{Schwerdtfeger}} = \frac{2k_{\text{ice}}\rho}{(3\rho_{\text{ice}} - \rho)}\,, \tag{12}$$

where ρ is in units $\mathrm{kg\,m^{-3}}$. Values on the dependency of thermal conductivity on relative firn density $D := \rho/\rho_{\text{ice}}$ were collected by Mellor (1977) and fitted by Schwander and others (1997)

$$k_{\text{Mellor}} = k_{\text{ice}} D^{2-0.5D}, \tag{13}$$

and the temperature dependent conductivity of ice is given in equation (10) and ρ is in units $\mathrm{kg\,m^{-3}}$. Still another parameterisation has been given by Sturm and others (1997)

$$k_{\text{Sturm}} = 0.138 - 1.01 \cdot 10^{-3}\rho + 3.233 \cdot 10^{-6}\rho^2\,. \tag{14}$$

All parameterisations of the thermal conductivity are shown in Figure 13. The values given by Schwerdtfeger are an upper limit, formulas of van Dusen and Sturm are at the lower limit. In the numerical models presented in this study, the average of the conductivities given in equations (11) and (12) has been used.

References

Alean, J., Haeberli, W., and Schädler, B. (1983). Snow accumulation, firn temperature and solar radiation in the area of the Colle Gnifetti core drilling site (Monte Rosa, Swiss Alps): distribution patterns and interrelationships. *Zeitschrift für Gletscherkunde und Glazialgeologie*, 19(2):131–147.

Blatter, H. (1987). On the thermal regime of an Artic valley glacier: a study of White Glacier, Axel Heiberg Island, N.W.T., Canda. *Journal of Glaciology*, 33(114):200–211.

Blatter, H. and Kappenberger, G. (1988). Mass balance and thermal regime of Laika ice cap, Coburg Island, N.W.T., Canada. *Journal of Glaciology*, 34(116):102–110.

Busslinger, A. (1998). *Geothermische Prognosen für tiefliegende Tunnel*. PhD thesis, ETH Zürich. Diss. ETH Nr. 12715.

Clauser, C. and Huenges, E. (1995). Thermal conductivity of rocks and minerals. In Ahrens, T., editor, *Rock Physics and Phase Relations*, volume 3 of *A Handbook of Physical Constants*, pages 105–126. American Geophysical Union.

Cocks, A. (1994). The structure of constitutive laws for the sintering of fine grained materials. *Acta Metallurgica et Materialia*, 42(7):2191–2210.

de Angelis, M. and Gaudichet, A. (1991). Saharan dust deposition over Mont Blanc (French Alps) during the last 30 years. *Tellus*, 43(B1):61–75.

Döscher, A., Gäggeler, H. W., Schotterer, U., and Schwikowski, M. (1996). A historical record of ammonium concentrations from a glacier in the Alps. *Geophysical Research Letters*, 23(20):2741–2744.

Duva, J. M. and Crow, P. D. (1994). Analysis of consolidation of reinforced materials by power law creep. *Mechanics of Materials*, 17:25–32.

Funk, M., Echelmeyer, K., and Iken, A. (1994). Mechanisms of fast flow in Jakobshavns Isbrae, Greenland; Part II: Modeling of englacial temperatures. *Journal of Glaciology*, 40(136):569–585.

Gagliardini, O. and Meyssonnier, J. (1997). Flow simulation of a firn-covered cold glacier. *Annals of Glaciology*, 24:242–248.

Haeberli, W. and Alean, J. (1985). Temperature and accumulation of high altitude firn in the Alps. *Annals of Glaciology*, 6:161–163.

Haeberli, W. and Funk, M. (1991). Borehole temperatures at the Colle Gnifetti core drilling site (Monte Rosa, Swiss Alps). *Journal of Glaciology*, 37(125):37–46.

Hutter, K. (1983). *Theoretical glaciology; material science of ice and the mechanics of glaciers and ice sheets*. D. Reidel Publishing Company/Tokyo, Terra Scientific Publishing Company.

Lliboutry, L. A. (1993). Internal melting and ice accretion at the bottom of temperate glaciers. *Journal of Glaciology*, 39(131):50–64.

Lüthi, M. (1999). *Experimental and numerical investigation of a firn covered cold glacier and a polythermal ice stream: Case studies at Colle Gnifetti and Jakobshavns Isbrae (Diss. ETH 13406)*. PhD thesis, ETH Zürich.

Lüthi, M. and Funk, M. (2000). Dating ice cores from a high Alpine glacier with a flow model for cold firn. *Annals of Glaciology*, 31:69–79.

Malvern, L. E. (1969). *Introduction to the Mechanincs of a Continuous Medium*. Prentice-Hall Series in Engineering of the Physical Sciences. Prentice-Hall, Inc.

MARC (1997). *MARC/MENTAT User's Manual*. MARC Analysis Research Corporation, 260 Sheridan Avenue, Palo Alto, CA 94306, K7 edition.

Margreth, S. and Funk, M. (1999). Hazard mapping for ice and combined snow/ice avalanches - two case studies from the Swiss and Italian Alps. *Cold Regions Science and Technology*, 30:159–173.

Medici, F. and Rybach, L. (1995). *Geothermal Map of Switzerland 1995 (Heat Flow Density)*. Studentendruckerei, Zürich.

Mellor, M. (1977). Engineering properties of snow. *Journal of Glaciology*, 19(81):15–66.

Oeschger, H., Schotterer, U., Stauffer, B., Haeberli, W., and Röthlisberger, H. (1977). First results from Alpine core drilling projects. *Zeitschrift für Gletscherkunde und Glazialgeologie*, 13(1-2):193–208.

Paterson, W. S. B. (1994). *The Physics of Glaciers*. Pergamon, New York, third edition.

Röthlisberger, H. (1981). Eislawinen und Ausbrüche von Gletscherseen. In *P. Kasser (Ed.), Gletscher und Klima - glaciers et climat, Jahrbuch der Schweizerischen Naturforschenden Gesellschaft, wissenschaftlicher Teil 1978*, pages 170–212. Birkhäuser Verlag Basel, Boston, Stuttgart.

Röthlisberger, H. (1987). Sliding phenomena in a steep section of Balmhorngletscher, Switzerland. *Journal of Geophysical Research*, 92(B9):8999–9014.

Rybach, L. and Pfister, M. (1994). Temperature predictions and predicive temperatures in deep tunnels. *Rock mechanics and rock engineering*, 27(2):77–88.

Schotterer, U., Oeschger, H., Wagenbach, D., and Münnich, K. O. (1985). Information on paleo–precipitation on a high–altitude glacier, Monte Rosa, Switzerland. *Zeitschrift für Gletscherkunde und Glazialgeologie*, 21:379–388.

Schüepp, M. (1961). *Klimatologie der Schweiz, C Lufttemperatur 2. Teil*. Beiheft zu den Annalen der MZA, Jg. 1960.

Schwander, J., Sowers, T., Barnola, J.-M., Blunier, T., Fuchs, A., and Malaizé, B. (1997). Age scale fo the air in the summit ice: Implication for glacial-interglacial temperature change. *Journal of Geophysical Research*, 102(D16):19'483–19'493.

Schwikowski, M., Brütsch, S., Gäggeler, H., and Schotterer, U. (1999a). A high-resolution air chemistry record from an Alpine ice core: Fiescherhorn glacier, Swiss Alps. *Journal of Geophysical Research*, 104(D11):13709–13719.

Schwikowski, M., Döscher, A., Gäggeler, H., and Schotterer, U. (1999b). Anthropogenic versus natural sources of atmospheric sulphate form an Alpine ice core. *Tellus*, 51B(5):938–951.

SMA-Annalen (1864–1999). *Annalen der Schweizerischen Meteorologischen Anstalt*. Zürich.

Sofronis, P. and McMeeking, R. M. (1992). Creep of power-law material containing spherical voids. *Journal of Applied Mechanics*, 59(2):S88–S95.

Sturm, M., Holmgren, J., König, M., and Morris, K. (1997). The thermal conductivity of seasonal snow. *Journal of Glaciology*, 43(143):26–41.

Vincent, C., Vallon, M., Pinglot, J., Funk, M., and Reynaud, L. (1997). Snow accumulation and ice flow at Dôme du Goûter (4300 m), Mont Blanc, French Alps. *Journal of Glaciology*, 43(145):513–521.

von Rudloff, H. (1980). Die Klimaentwicklung in den letzten Jahrhunderten im mitteleuropäischen Raume (mit einem Rückblick auf die postglaziale Periode). In Oeschger, H., Messerli, B., and Svilar, M., editors, *Das Klima: Analysen und Modelle, Geschichte und Zukunft*, pages 125–148. Springer Verlag.

Wagenbach, D., Münnich, K. O., Schotterer, U., and Oeschger, H. (1988). The anthropogenic impact on snow chemistry at Colle Gnifetti, Swiss Alps. *Annals of Glaciology*, 10:183–187.

Wegmann, M. (1998). Frostdynamik in hochalpinen Felswänden am Beispiel der Region Jungfraujoch–Aletsch. Mitteilung 161, Versuchsanstalt für Wasserbau, Hydrologie und Glaziologie der ETH Zürich.

Wegmann, M., Gudmundsson, G. H., and Haeberli, W. (1998). Permafrost changes in rock walls and the retreat of Alpine glaciers — thermal modelling approach. *Permafrost and Periglacial Processes*, 9:23–33.

Zienkiewicz, O. C. and Taylor, R. L. (1989). *The Finite Element Method*. McGraw-Hill Book.

Figure captions

Fig. 1: Surface elevation map of Colle Gnifetti. The thick line indicates the border of the 3D model and points mark the drill sites. Boreholes reached near bedrock at depths of $124\,\mathrm{m}$ (B82-1), $66\,\mathrm{m}$ (B82-2), $61\,\mathrm{m}$ (B95-1) and $101\,\mathrm{m}$ (B95-2). Boreholes B76 ($33\,\mathrm{m}$) and B77 (55 and $65\,\mathrm{m}$) stopped far above bedrock. Coordinates are in meters and correspond to the official Swiss coordinate system, contour lines indicate the altitude above sea level. The location of the flowline model is marked with a thick dashed line.

Fig. 2: Temperatures measured in three boreholes on Colle Gnifetti are plotted in the left frames. Temperatures in boreholes B95-1 and B95-2 were measured in 1996/97, those of B82-1 in 1983 (data for B82-1 from Haeberli and Funk, 1991). Heat fluxes are calculated from measured temperature gradients and the density dependent thermal conductivities.

Fig. 3: Modelled velocity field from the flowline model. Little flags indicate the position of stakes. The measured velocities are indicated with black arrows, modelled velocities are drawn in gray. Note the unusual shape of the velocity profiles with an increase of horizontal velocities near the surface. This is an effect of the low viscosity of the firn layer. Temperature profiles were measured in boreholes B95-1 and B95-2, indicated with thick vertical lines.

Fig. 4: The model geometry and applied boundary conditions of the heat flow model. Only the uppermost part of the model is shown (the geometry extends down to sea level). The shaded area annotated 'Glacier' identifies the glacier flow model geometry (Figure 3) and thus the part of the model where advection is operative.

Fig. 5: Modelled steady state temperature profiles. Note the different curvature of the profiles.

Fig. 6: The surface temperature variation prescribed in the transient model runs. The temperature curve is doubly smoothed over a 9 year period. Steady conditions are assumed for the time prior to the year 800. The right panel shows a closeup of the last part of the prescribed history and two future scenarios: steady temperatures (dashed line) or a linear increase of $1^{\circ}\mathrm{C}$ during the next 50 years (solid line).

Fig. 7: Modelled englacial temperatures in 1997 (thick solid line) from the transient model are compared to measured temperatures (dots and triangles). Thin solid lines indicate the modelled temperatures in 1996. The 1982 temperature profile is similar to a steady state profile (dashed line, same as in Figure 5).

Fig. 8: Contour lines of modelled temperatures in 1997 from the transient model including the effects of latent heat. The glacier geometry is indicated by a shaded area. The arrow indicates the location of the profiles plotted in Figure 9.

Fig. 9: Profiles of temperature and heat flux taken at the horizontal coordinate $300\,\mathrm{m}$ (indicated with an arrow in Figure 8). a) Modelled temperatures from the transient model including the effects of latent heat at five different times. b) The modelled vertical heat flux strongly decreases at an altitude of $2900\,\mathrm{m}$ due to a thawing permafrost base. c) and d) Modelled temperature and vertical heat flux for dry rock (without phase transition).

Fig. 10: Englacial temperatures in borehole B 95-2 at depths of 15, 25 and $35\,\mathrm{m}$ from the transient model. The thick solid line indicates the prescribed surface temperature history (labelled 'surface'). The temperature at the base of the borehole is indicated with the uppermost solid line (labelled 'bed').

Fig. 11: Modelled future temperature profiles in borehole B 95-2 under the assumption of constant surface temperatures during the next 50 years. Thin lines show the modelled temperatures after time increments of ten years, the leftmost refers to the year 2000 and the thick line is the 1997 state (same curve as in Figure 7). The temperature inversion in borehole B95−2 is fading out after some 30 years and considerable basal warming takes place.

Fig. 12: Modelled future temperature profiles in borehole B 95-2 under a linear surface temperature increase of one degree during the next 50 years. The lines show the modelled temperatures after time increments of ten years, the thick line is the same as in Figure 7.

Fig. 13: The density dependence of the heat conductivity in firn as parameterised by several authors.

Fig 1

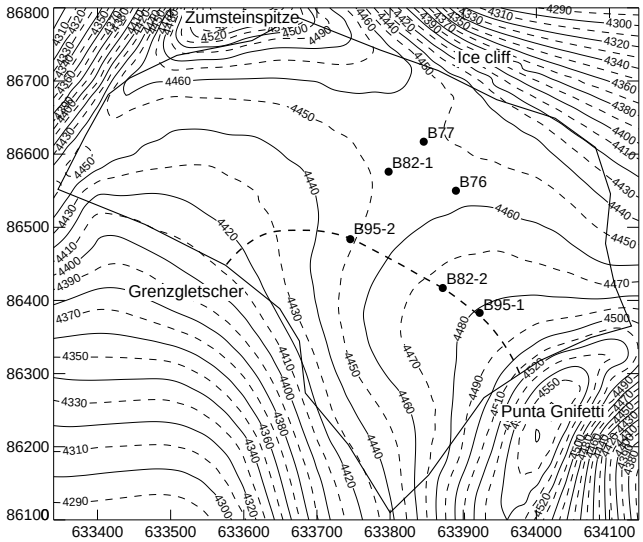
Zumsteinspitze
Ice cliff
B77
B82-1
B76
B95-2
B82-2
B95-1
Grenzgletscher
Punta Gnifetti
86800
86700
86600
86500
86400
86300
86200
86100
633400
633500
633600
633700
633800
633900
634000
634100

Fig 2

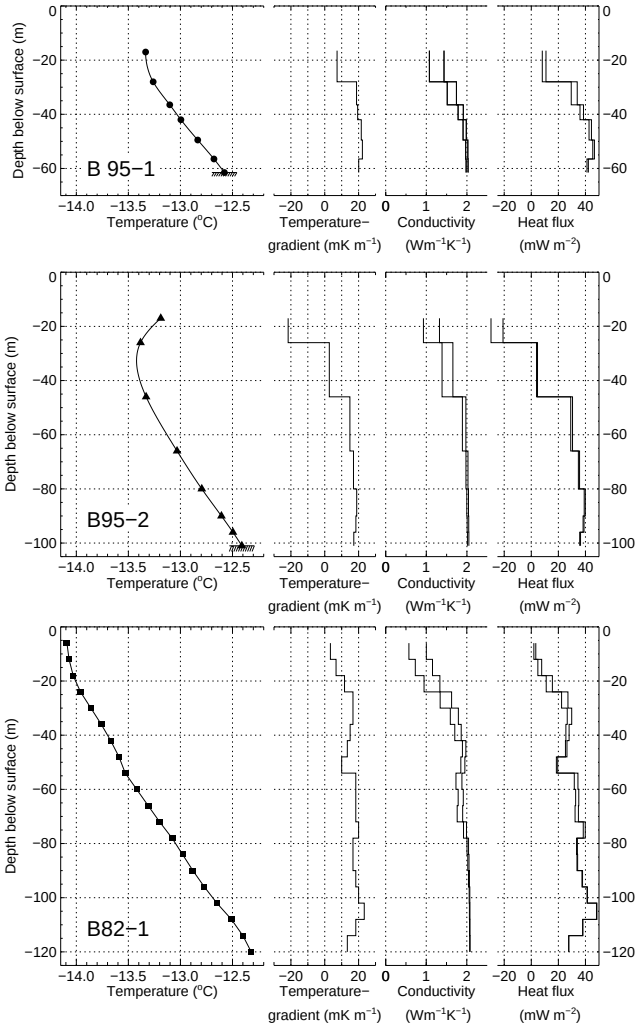
B 95−1
B95−2
B82−1
Depth below surface (m)
Temperature (°C)
Temperature−
gradient (mK m⁻¹)
Conductivity
(Wm⁻¹K⁻¹)
Heat flux
(mW m⁻²)

Fig 3

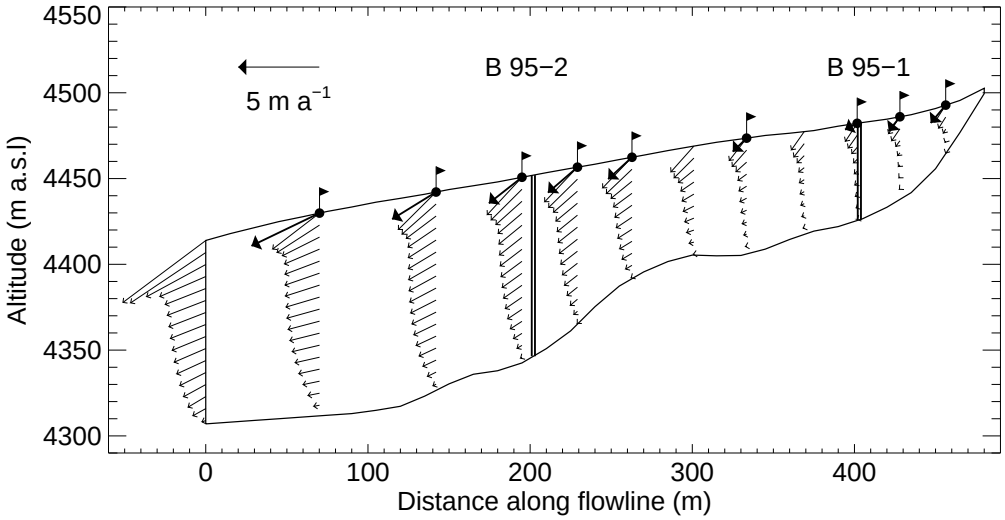
4550
4500
4450
4400
4350
4300
Altitude (m a.s.l)
5 m a^{-1}
B 95−2
B 95−1
0
100
200
300
400
Distance along flowline (m)

Fig 4

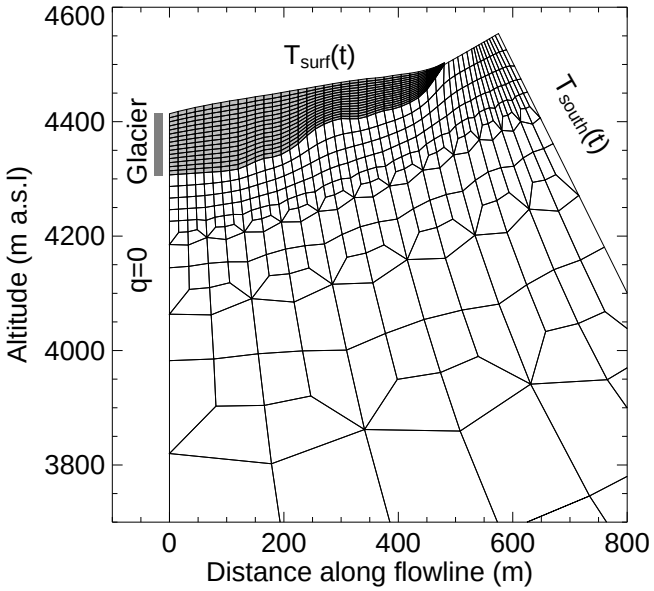
4600
4400
4200
4000
3800
Altitude (m a.s.l)
$T_{surf}(t)$
$T_{south}(t)$
Glacier
q=0
0
200
400
600
800
Distance along flowline (m)

Fig 5

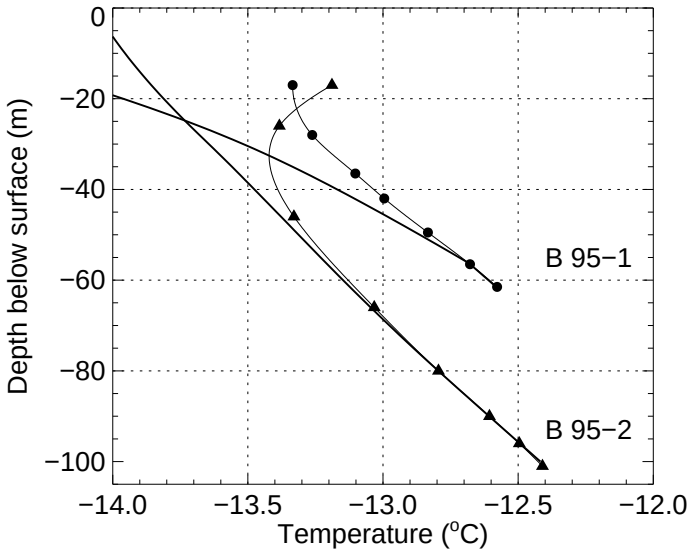
Depth below surface (m)
0
−20
−40
−60
−80
−100
−14.0
−13.5
−13.0
−12.5
−12.0
Temperature (°C)
B 95−1
B 95−2

Fig 6

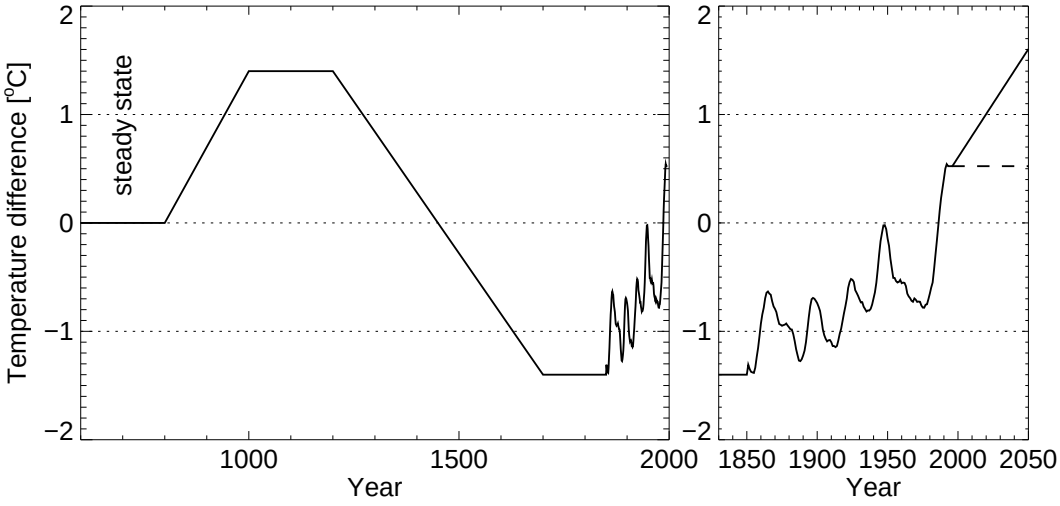
Temperature difference [°C]
steady state
2
1
0
−1
−2
1000
1500
2000
Year
1850
1900
1950
2000
2050
Year

Fig 7

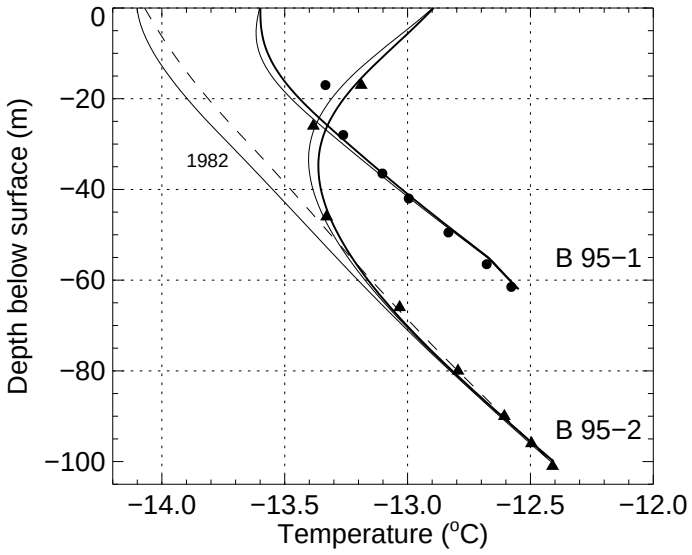
0
−20
−40
−60
−80
−100
Depth below surface (m)
1982
B 95−1
B 95−2
−14.0
−13.5
−13.0
−12.5
−12.0
Temperature (°C)

Fig 8

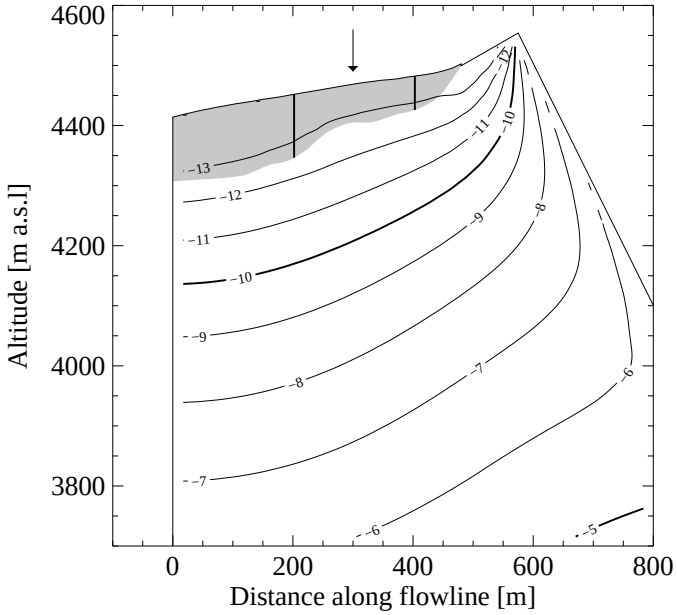
4600
4400
4200
4000
3800
Altitude [m a.s.l]
−13
−12
−11
−10
−9
−8
−7
−6
−5
0
200
400
600
800
Distance along flowline [m]

Fig 9

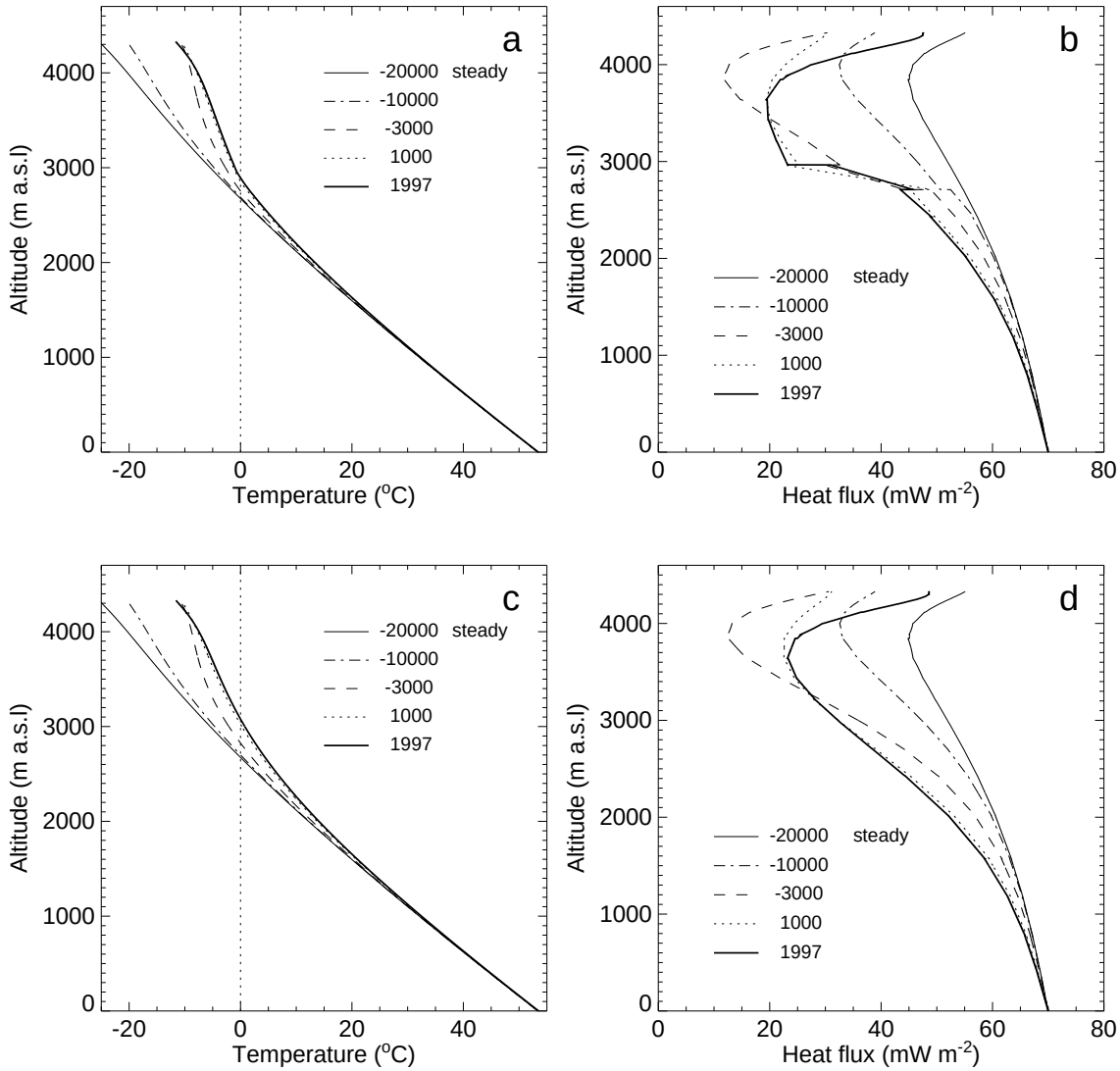
a
b
c
d
-20000 steady
-10000
-3000
1000
1997
Altitude (m a.s.l)
Temperature (°C)
Heat flux (mW m-2)
0
1000
2000
3000
4000
-20
0
20
40
60
80

Fig 10

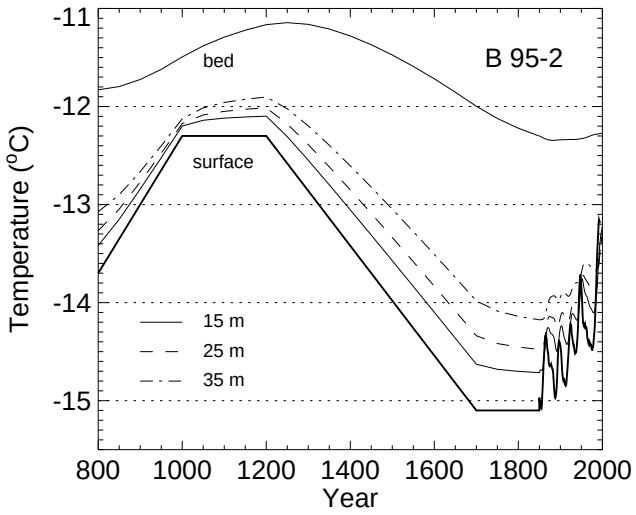
-11
-12
-13
-14
-15
bed
B 95-2
surface
15 m
25 m
35 m
Temperature (°C)
800
1000
1200
1400
1600
1800
2000
Year

Fig 11

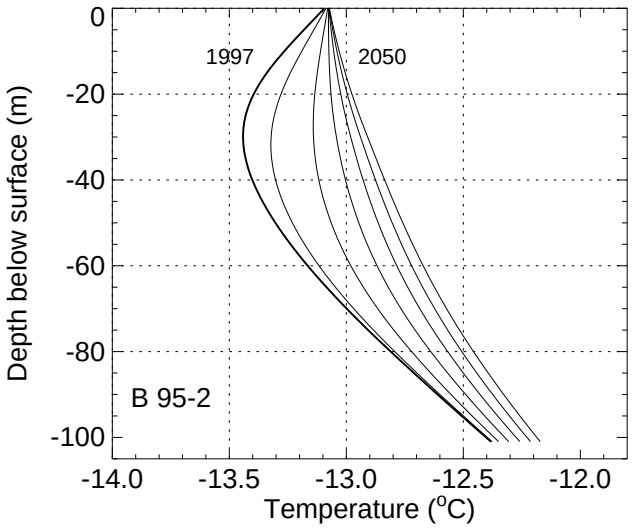
0
-20
-40
-60
-80
-100
1997
2050
B 95-2
Depth below surface (m)
-14.0
-13.5
-13.0
-12.5
-12.0
Temperature (°C)

Fig 12

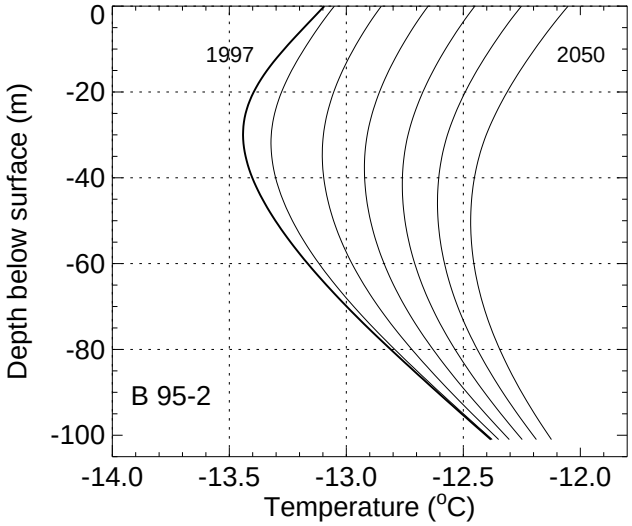
1997
2050
B 95-2
Depth below surface (m)
0
-20
-40
-60
-80
-100
-14.0
-13.5
-13.0
-12.5
-12.0
Temperature (°C)

Fig 13

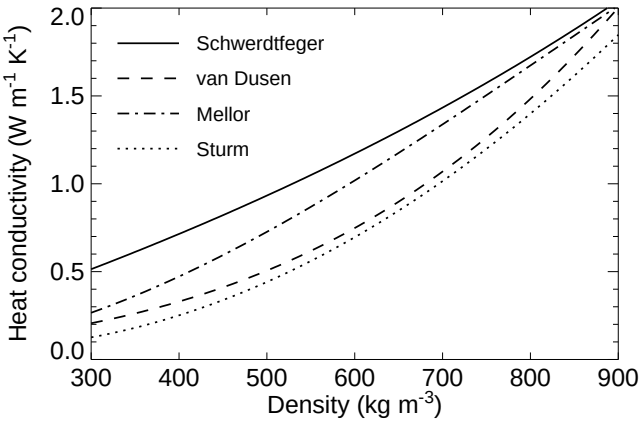
Schwerdtfeger
van Dusen
Mellor
Sturm
Heat conductivity (W m-1 K-1)
2.0
1.5
1.0
0.5
0.0
300
400
500
600
700
800
900
Density (kg m-3)